MECHANISM OF VERTICAL DISPLACEMENT EVENTS IN JT-60U DISRUPTIVE DISCHARGES

Y. NAKAMURA, R. YOSHINO, Y. NEYATANI,
T. TSUNEMATSU, M. AZUMI
Japan Atomic Energy Research Institute,
Naka Fusion Research Establishment,
Naka-machi, Naka, Ibaraki, Japan

N. POMPHREY, S.C. JARDIN
Princeton Plasma Physics Laboratory,
Princeton University,
Princeton, New Jersey,
United States of America

ABSTRACT. Enhanced vertical displacement events (VDEs), which are frequently observed in JT-60U disruptive discharges, are investigated using the Tokamak Simulation Code (TSC). The rapid plasma current quench can accelerate the vertical displacement, owing to both the up/down asymmetry of the eddy current distribution arising from the asymmetric geometry of the JT-60U vacuum vessel and the degradation of magnetic field decay index n, leading to high growth rates of positional instability. For a slightly elongated configuration ($n = -0.9$), the asymmetry of attractive forces on the toroidal plasma plays a dominant role in the VDE mechanism. For a more elongated configuration ($n = -1.7$), the degradation of field decay index n plays an important role on VDEs, in addition to the effect of asymmetric attractive forces. It is shown that the VDE characteristics of a highly elongated configuration with a rapid plasma current quench can be dominated by the field decay index degradation. It is also pointed out that both the softening of current quenches as was experimentally developed in the JT-60U tokamak, and the optimization of the allowable elongation of the plasma cross-section are critical issues in the development of a general control strategy of discharge termination.

1. INTRODUCTION

In investigating tokamak disruptions we seek to improve our understanding to the point where disruption-free discharges are realizable, or at least soft landing disruptions are achieved. Many experimental and theoretical works have sought this goal; however, no reliable control technique has yet been developed because of the complexity of disruptive processes, which can be device dependent. Typically, experimentally observed disruptive discharges show rapid plasma current decay (I_p quench) following an energy quench, a coincident fast plasma displacement (a vertical displacement event (VDE)) and a shrinking plasma boundary [1–3]. A rapid I_p quench induces large eddy currents in the vacuum vessel, increasing the electromagnetic forces [4, 5] and making the position control of a plasma difficult. A VDE can cause serious wall damage since any active feedback becomes incapable of maintaining position control during the disruption process, and the unstable plasma with high internal energy can hit plasma-facing components in the vacuum vessel. A VDE also causes a large halo current with a large vertical shift of the unstable plasma, and results in substantial electromagnetic forces on structural components that can be larger than those caused by the usual eddy current. VDEs are especially troublesome in machines with non-circular plasma cross-sections like JET and JT-60U, and it is commonly recognized that VDEs are intimately linked with vertically elongated tokamaks [3]. In recent years, major experiments in tokamak research have been directed towards vertically elongated plasmas like JT-60U, DIII-D and JET, because such highly elongated plasmas have benefits for improved confinement leading to high beta. It is also well known that shaping the tokamak cross-section allows one to increase the total plasma current. However, elongated plasmas have the drawback of positional instability. From the point of view of tokamak conducting structure, design and shape optimization of the plasma cross-section understanding positional instabilities and VDEs is essential for the success of next generation tokamak fusion devices like ITER [6]. To improve the reliability of tokamak fusion reactors, both rapid I_p quenches and fast VDEs in disruptive discharge termination must be avoided.

Systematic investigations on the amelioration of disruptions have been carried out in ASDEX Upgrade, in which several strategies were developed to protect the tokamak by avoiding dangerous plasma events, and significant contributions were made to disruption studies [6]. In order to soften the disruption, the current quenches frequently caused by density limit disruptions have been investigated in JT-60U divertor plasmas [1]. It was clarified that softening the energy quench is a possible method of softening the I_p quench. Moreover, it was experimentally demonstrated that reducing the impurity influxes in an energy quench and direct neutral beam (NB) heating of the plasma core during an I_p quench are beneficial for reducing the speed of the I_p quench. Parallel to this progress, one of the authors (R.Y.) showed experimentally a close relation between the I_p quench rate and the VDE rate; a rapid I_p quench enhances the VDE [3]. However, despite this progress in understanding what controls the speed of I_p quench rates, all the VDE mechanisms during disruption have not been clearly identified and a general method for avoiding or controlling VDEs has not yet been proposed.

With regard to VDEs, vertical displacements were observed to be much faster during rapid I_p quenches in JT-60U disruptive discharge experiments [3] than observed in JET [7]. The experimental growth rates of VDEs becomes 3 or more times higher than the values predicted by positional stability theory, including the stabilizing effect of the JT-60U vacuum vessel. Control methods cannot suppress VDEs during a disruptive process because of insufficient available control gain of the feedback loop. Wall damage could become very serious in future tokamaks like ITER unless a reliable control technique is developed. There are many possible candidate mechanisms to describe the JT-60U observation of fast VDEs, for example, peaking of the plasma current profile, shrinkage of the plasma cross-section [8], imbalance of attractive forces due to up/down asymmetry of the equilibrium configuration, and some destabilizing effects of the vacuum vessel current [6]. On the contrary, halo currents that appear in the open flux scrape-off layer (SOL), especially in the last half phase of the disruption process, are believed to suppress VDEs [2, 9].

In this paper, we describe in detail the VDE mechanism in JT-60U I_p quenches especially focusing on the first half phase of the disruption process, i.e. the halo current-free phase [9]. The disruptive discharges that we will discuss in this paper are initiated by density limit disruptions. The main plasma parameters are plasma current I_p =1.5 MA, elongation κ = 1.3–1.6 and relatively low beta ohmically heated plasmas with $\beta_p < 0.2$, and the plasma shape is a bottom-diverted single-null (SN) configuration. To clarify the VDE mechanism, first, the fundamental characteristics of JT-60U positional stability and, second, the non-linear evolution of plasma displacement interacting with the eddy currents on the vacuum vessel are studied numerically using the TSC code [10]. The JT-60U vacuum vessel, which plays an important role in stabilizing the vertical instability, was carefully modelled using an assembly of multifilaments to reproduce the realistic L/R time and geometry [11]. Self-consistent TSC simulations of JT-60U plasma disruptions were carried out, including the stabilizing effect of the vacuum vessel. The linear growth rate of positional instability keeping the plasma current constant in time was evaluated, and its dependence on both the magnitude of the field decay index

$$n = R/B_Z(\partial B_R/\partial Z) = -R/B_Z(\partial B_Z/\partial R)$$

(related to the elongation κ) and the initial Z position of the magnetic axis was clarified. The relation of the plasma current profile shape to the linear growth rate, which reflects the effective plasma–wall distance, was also evaluated quantitatively. Experimentally observed VDEs were reproduced quite well by the TSC simulations. Comparative studies of the elongated configuration (κ = 1.6) and the standard configuration (κ = 1.3) in JT-60U were made. It is found that the enhancement of magnetic field curvature, i.e. the degradation of the field decay index, due to induced eddy currents set up by the rapid I_p quench, can accelerate VDEs, and this new mechanism must be added to the list of previously proposed mechanisms [6]. This suggests guidelines for the design criteria for next generation tokamaks, where it is necessary to determine the allowable elongation without either fast VDEs or hard disruptions. The allowable configuration could be limited by the sacrifice of favourable elongation of the plasma cross-section.

The following sections describe the basic equations of the TSC model, the modelling of the JT-60U tokamak (both in Section 2), fundamental characteristics of JT-60U positional stability (in Section 3) and JT-60U experiments on disruptive discharges and mechanisms of fast VDE, during I_p quench (in Section 4). Finally, conclusions are given (in Section 5).

2. TSC MODELLING OF THE JT-60U TOKAMAK

TSC [10] is the numerical code that is able to model the behaviour of a free-boundary axisymmetric tokamak plasma interacting with a conducting wall and a set of axisymmetric conductors that obey circuit equations with active feedback amplifiers included. Modified magnetohydrodynamic equations are solved inside a computational domain that includes a plasma region, a vacuum region, a specified number of solid conductors and a wall. The interaction of the plasma with passive conducting structures is treated in a self-consistent manner. TSC has been applied to many problems in tokamak design and has been used to simulate experiments on various toroidal fusion devices [2, 4, 5, 12–14].

Here, we describe the TSC numerical model and details of the modelling of VDEs in the JT-60U tokamak in order to reveal typical features of the VDE mechanism. The assumptions and simplifications utilized in our computational work are also discussed.

2.1. Basic equations of axisymmetric plasma evolution

TSC uses an inertial enhancement technique to solve the plasma force balance equation,

$$\frac{\partial \boldsymbol{m}}{\partial t} + \boldsymbol{F}_{\mathrm{v}}(\boldsymbol{m}) = \boldsymbol{J} \times \boldsymbol{B} - \nabla p \tag{1}$$

Here, $\boldsymbol{m}$ is the plasma momentum density $M_{\mathrm{i}} n \boldsymbol{v}$, which is expressed in terms of a stream function A, a toroidal component ω and a potential Ω:

$$\boldsymbol{m} = \nabla\phi \times \nabla A + \omega \nabla\phi + \nabla\Omega \tag{2}$$

where ϕ is the toroidal angle. Instead of the convective derivative term, a specific form of the plasma viscosity operator,

$$\boldsymbol{F}_{\mathrm{v}}(\boldsymbol{m}) = -\nu_1[\nabla^2 \boldsymbol{m} - \nabla(\nabla \cdot \boldsymbol{m})] - \nu_2 \nabla(\nabla \cdot \boldsymbol{m}) \tag{3}$$

is introduced artificially on the left hand side of Eq. (1). The mass M_{i} and the viscosities ν_1 and ν_2 are assigned enhanced values to make the time integration feasible while keeping the left hand side of Eq. (1) small compared with the terms on the right hand side. In order to obtain physically correct results, the TSC model must nearly satisfy the static equilibrium condition: $\boldsymbol{J} \times \boldsymbol{B} = \nabla p$, with an integration time step that is much longer than the Alfvén time-scale. It must be verified a posteriori that the effect of the modified inertial terms is small and that the physical results are independent of the fictitious mass and viscosity values. In order to confirm the TSC results, we repeat the simulations with smaller mass enhancement factors to ensure proper convergence.

The magnetic field is expressed in axisymmetric toroidal geometry with symmetry angle ϕ as

$$\boldsymbol{B} = \nabla\phi \times \nabla\Psi + g\nabla\phi \tag{4}$$

in terms of the poloidal flux per radian Ψ and the toroidal field function g. The modified force balance equation (1) can be rewritten in the following scalar forms:

$$\frac{\partial}{\partial t}\nabla^2\Omega + \nabla \cdot \left(\frac{\Delta^*\Psi}{\mu_0 x^2}\nabla\Psi + \frac{g}{\mu_0 x^2}\nabla g + \nabla p - \nu_2 \nabla(\nabla^2\Omega) \right) = 0 \tag{5a}$$

$$\frac{\partial}{\partial t}\Delta^* A + x^2 \nabla \cdot \left(\frac{\Delta^*\Psi}{\mu_0 x^2}\nabla\Psi \times \nabla\phi + \frac{g}{\mu_0 x^2}\nabla g \times \nabla\phi + \frac{\nu_1}{x^2}\nabla(\Delta^* A) \right) = 0 \tag{5b}$$

$$\frac{\partial}{\partial t}\omega + \mu_0^{-1} \nabla\phi \times \nabla g \cdot \nabla\Psi - \nu_1 \Delta^* \omega = 0 \tag{5c}$$

where $\Delta^* \equiv x^2 \nabla \cdot (x^{-2}\nabla)$ is the standard toroidal elliptic operator and x is the radius in the cylindrical co-ordinates. If we consider the static solution of Eq. (5) with zero viscosities, these equations are exactly equivalent to the well known Grad–Shafranov equation,

$$\Delta^*\Psi + \mu_0 x^2 \frac{\mathrm{d}}{\mathrm{d}\Psi} p(\Psi) + \frac{1}{2}\frac{\mathrm{d}}{\mathrm{d}\Psi} g^2(\Psi) \equiv 0 \tag{6}$$

Faraday's law and Ohm's law,

$$\boldsymbol{E} + \boldsymbol{v} \times \boldsymbol{B} = \boldsymbol{R} \tag{7}$$

where $\boldsymbol{R}$ contains the non-ideal terms, yield evolution equations for the poloidal flux and toroidal field functions,

$$\frac{\partial\Psi}{\partial t} + \frac{1}{\rho_0}(\nabla\phi \times \nabla A \cdot \nabla\Psi + \nabla\Omega \cdot \nabla\Psi) = x^2 \nabla\phi \cdot \boldsymbol{R} \tag{8}$$

$$\frac{\partial g}{\partial t} + x^2 \nabla \cdot \left(\frac{g}{\rho_0 x^2}(\nabla\phi \times \nabla A + \nabla\Omega) - \frac{\omega}{\rho_0 x^2}\nabla\phi \times \nabla\Psi - \nabla\phi \times \boldsymbol{R} \right) = 0 \tag{9}$$

Here, $\rho_0 \equiv n_0 M_i$ is the enhanced mass density. The non-ideal dissipation vector $\boldsymbol{R}$ in Eq. (7) is given by

$$\boldsymbol{R} \equiv \eta_{\parallel} \boldsymbol{J} \tag{10}$$

with $\eta_{\parallel} \equiv 0.51 \times 10^{-4}\, Z_{\mathrm{eff}} (\ln \Lambda) T_e^{-3/2}$ (T_e is in electronvolts). Z_{eff} is the effective nuclear charge. Thus, the terms that involve $\boldsymbol{R}$ in Eqs (8) and (9) can be written as

$$x^2 \nabla\phi \cdot \boldsymbol{R} = \frac{\eta_{\parallel}}{\mu_0} \Delta^* \Psi \tag{11}$$

and

$$\nabla\phi \times \boldsymbol{R} = \frac{\eta_{\parallel}}{\mu_0} \nabla g \tag{12}$$

In our TSC model, the plasma pressure p is always assumed to be given as the prescribed surface quantity $p(\Psi)$. Allowing for the possibility of an applied voltage $V(t)$ to an external circuit, the circuit equation of the poloidal flux Ψ_n at the nth poloidal field coil is given by

$$\frac{\partial \Psi_n}{\partial t} = \frac{\eta_n}{\mu_0} \Delta^* \Psi_n + \frac{1}{2\pi} V_n(t) \tag{13}$$

where V_n is the voltage of the power supply. For a passive conducting structure such as a vacuum vessel, the external voltage $V(t)$ is set to zero.

At the computational domain boundary $\boldsymbol{x}_b$, i.e. the outer boundary of the vacuum region, the toroidal field strength g and the poloidal flux Ψ are given as

$$g(\boldsymbol{x}_b) = g_0 = \frac{\mu_0}{2\pi} I_{\mathrm{TF}} \tag{14}$$

$$\Psi(\boldsymbol{x}_b, t) = \frac{\mu_0}{2\pi} \int_p G(\boldsymbol{x}_b; \boldsymbol{x})\, J_\phi(\boldsymbol{x}, t)\, \mathrm{d}^2 \boldsymbol{x} + \sum_{i=1}^{N} \frac{\mu_0}{2\pi} G(\boldsymbol{x}_b; \boldsymbol{x}_i) I_i \tag{15}$$

Here, I_{TF} is the total current in all the toroidal field coils, $G(\boldsymbol{x}_b; \boldsymbol{x})$ is the Green's function for an axisymmetric current filament $\Delta^* G = 2\pi\delta(\boldsymbol{x} - \boldsymbol{x}')$ and J_ϕ is the toroidal component of plasma current. In TSC, the vacuum region is modelled as a cold and low density plasma, and the boundary condition on the plasma momentum density is set to be

$$\nabla \cdot \boldsymbol{m} = 0, \qquad \boldsymbol{m} \cdot \boldsymbol{n} = 0 \tag{16}$$

2.2. The TSC model of JT-60U

Here, we describe the TSC modelling of the JT-60U tokamak and discuss the validity of our simplifying assumptions for the TSC computational study.

The TSC model can accurately compute the full non-linear axisymmetric and deformable motion including realistic control aspects, such as an active feedback system, resistive conductors, and circuit and power supply dynamics. However, we focus on the axisymmetric dynamics of the toroidal plasma interacting only with the eddy current on the vacuum vessel, because the purpose of this paper is to clarify the VDE mechanism during a tokamak current quench. During the VDE, the coupling of the plasma with all the poloidal field coil systems is neglected and the poloidal field coils are assumed to provide only the static magnetic field to keep the initial plasma equilibrium, i.e. we neglected both the active feedback and the passive response of the poloidal field coil system. The validity of this simplification is justified by the JT-60U experimental evidence especially during the first half phase of the VDE (< 10 ms) in disruptive discharges.

The inclusion of the details of plasma transport, including impurity influx and degradation of energy confinement, is beyond the scope of the computational work in this paper. The functional forms of the plasma pressure profile and plasma density profile are assumed to be unchanged during the TSC simulation. These are given by $p(\overline{\Psi}) = p_0 \overline{\Psi}^{3/2}$ and $n(\overline{\Psi}) = n_0 \overline{\Psi}^{1/2}$, respectively. Here, $\overline{\Psi}$ $(= (\Psi - \Psi_s)/(\Psi_{\mathrm{axis}} - \Psi_s))$ is the normalized poloidal flux. The magnitudes of the pressure and density are treated as being given and correspond to low $\beta_p (< 0.2)$.

Although the TSC results include the effects of plasma deformation, we will discuss the plasma trajectory mainly in terms of the position of the magnetic axis and the value of the plasma current. When necessary, other physical parameters, such as internal inductance ℓ_i, elongation κ and triangularity δ, will be shown explicitly. In some situations, especially in highly elongated tokamaks, the effect of deformation is believed to be essential, and the effects of plasma deformability on the feedback stabilization of axisymmetric modes have been studied in great detail [15, 16]. The significant results are that plasmas with strongly shaped cross-sections, for example $\kappa = 2.0$, have unstable motion different from a rigid shift, i.e. the true unstable motion of highly elongated tokamak plasmas involves non-rigid deformations [15], which

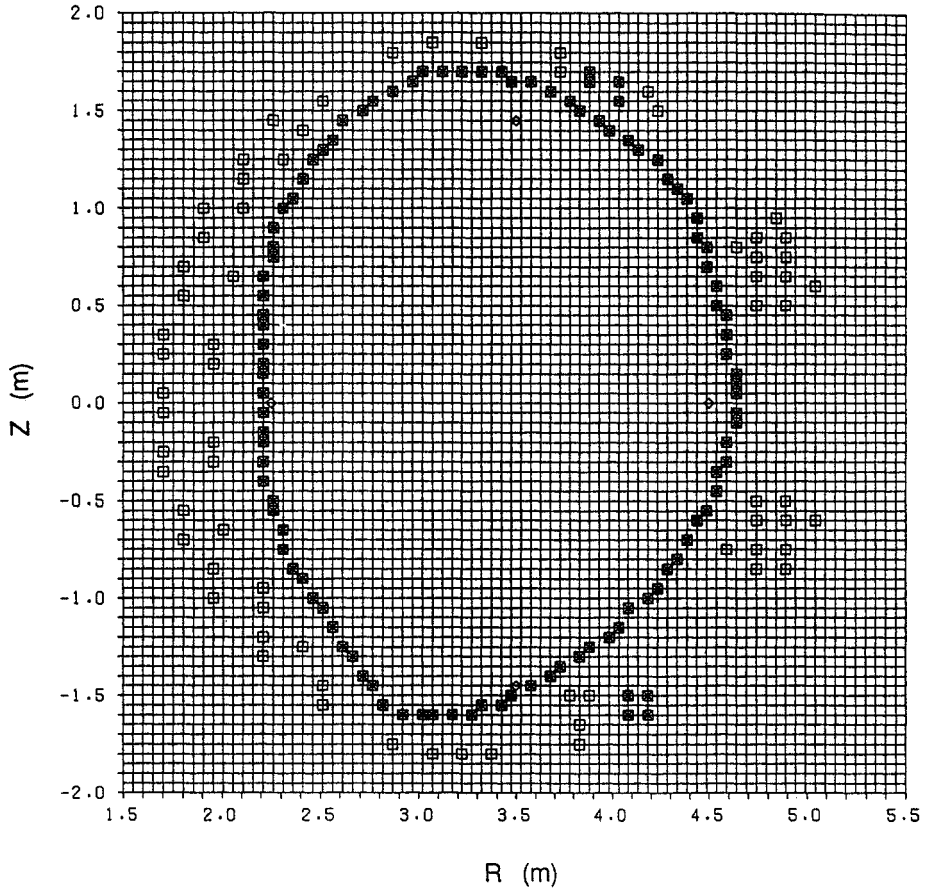

FIG. 1. TSC computational domain and configurations of JT-60U poloidal field coil systems and vacuum vessel: egg shaped and slightly up/down asymmetric conducting structures indicate the vacuum vessel, which is represented by a discretized array of 100 elements. The dominant up/down antisymmetric current mode of the vacuum vessel has a decay time constant of about 8 ms. The coil series outside the vacuum vessel consists of the poloidal field coil systems. An inside limiter was placed at R = *2.22 m. The computational domain is the square box from 1.5 m to 5.5 m in the major radius direction and from −2.0 m to 2.0 m in the vertical direction. This domain is divided into 80 × 80 grids with equal spacings of 5 cm. JT-60U can be operated with two different configurations with* n = *−0.9 and* n = *−1.7 by switching the mechanical connections of the vertical field coil system.*

can adversely affect the ability of a feedback system to stabilize the plasma motion regardless of the optimized gain of the feedback system [15]. Experimental results [17] have indicated that the optimization of plasma shape in DIII-D may be limited by the difficulties of detecting and controlling a significant non-rigid component of the plasma motion. Notwithstanding the importance of plasma deformability, we will not place special interest on deformation, since the nominal configuration of the JT-60U tokamak is characterized by mild elongations of κ = 1.3-1.6 and δ = 0.0–0.1, and the effects of deformation are less important.

It has been pointed out that the plasma halo current, which flows both toroidally and poloidally in the SOL region just outside the main plasma (halo region), significantly affects plasma dynamics for DIII-D disruptive discharges [2]. Although the temperature in the low density halo region is relatively low (a few electronvolts), a large electric field is produced by a vertical plasma shift, by diamagnetic flux changes due to rapid loss of thermal energy and by decaying plasma current. This electric field may produce the force-free currents that flow along open field lines, intersect conductors, flow along minimum impedance paths and return to the halo region.

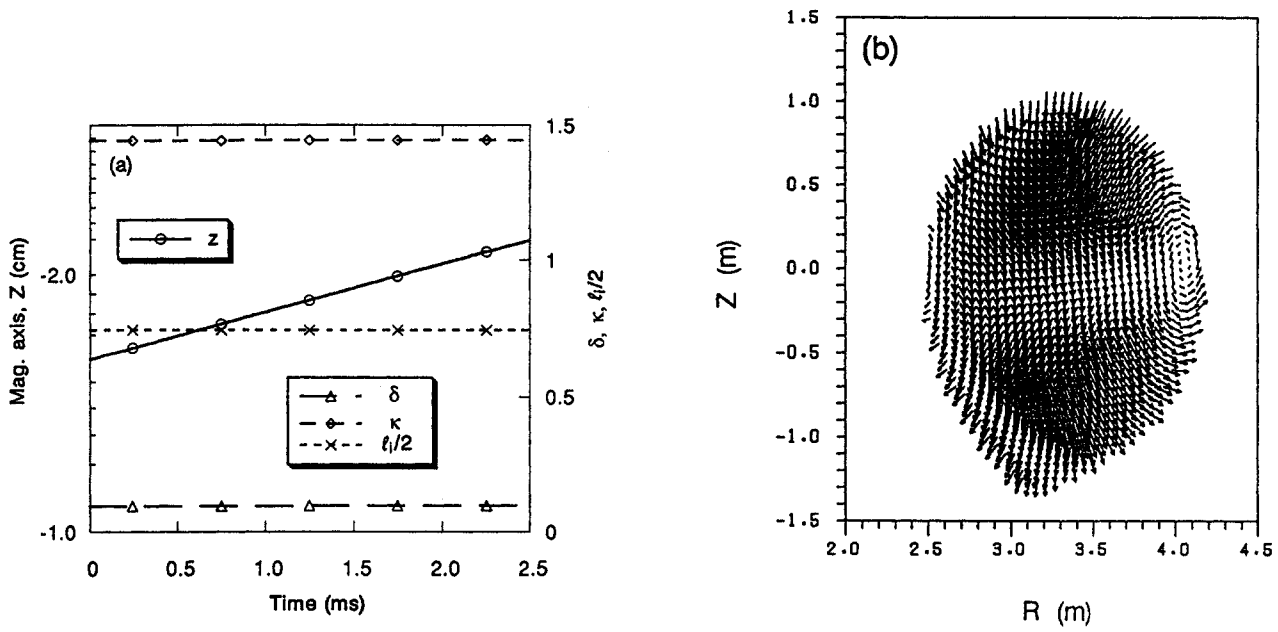

FIG. 2. Typical TSC simulation of time evolution of JT-60U positional instability (n = −1.7, I_p = 1.5 MA, R = 3.33 m). *(a) Vertical displacement of magnetic axis (open circles), elongation (open diamonds) and triangularity (open triangles) and* $\ell_i/2$ *(crosses) versus time. The vertical displacement of the magnetic axis evolves as an almost pure exponential growth from the initial position of* Z = 1.6 cm. *(b) Snapshot of 2-D vector field of poloidal plasma velocity at 2.0 ms. In JT-60U, the dominant mode of the vertical displacement is an almost uniform rigid shift and the deformation can be neglected.*

Observations [18, 19] of DIII-D and JET disruptions indicate that up to 20–30% of the initial plasma current may flow between the halo region and the vacuum vessel. These poloidal halo currents can lead to vertical vessel forces that are larger in magnitude than the forces from the usual toroidal eddy currents. A large amount of halo current appears mainly in the last half phase of plasma current termination after the large vertical shift of the magnetic axis. JT-60U measurements show no evidence of halo current in the first half phase of disruptions [9]. This result clearly shows that halo currents do not play an important role in VDEs on JT-60U, especially in the first half phase of the disruption. Therefore, in this paper, we neglect the effect of halo current on VDEs.

JT-60U is a vertically elongated, bottom-diverted SN tokamak. The parameters of JT-60U are the following: the maximum plasma current achieved is 5 MA, the maximum toroidal magnetic field is 4.4 T, the average plasma minor radius is 0.8 to 1.1 m and the plasma major radius is 3.0 to 3.6 m. JT-60U can be operated with two different configurations, with vertical field decay indices $n = -0.9$ and $n = -1.7$, by switching the mechanical connections of the vertical field coil system. Figure 1 illustrates the TSC computational domain and the nominal conductors that model the JT-60U poloidal field coil systems and the vacuum vessel. The egg shaped and slightly up/down asymmetric vacuum vessel is represented by a discretized array of 100 elements, each of whose resistances and self-inductances are specified to match the local value of the toroidal path of the actual vacuum vessel [11]. The dominant up/down antisymmetric current mode of the vacuum vessel, which stabilizes vertical displacement, has a decay time constant of about 8 ms, while the nominal horizontal field coil L/R time is about 280 ms. The computational domain is the square box with 1.5 to 5.5 m in the major radius direction and −2.0 to 2.0 m in the vertical direction. This domain is divided into 80×80 grids with equal spacings of 5 cm. An inside limiter was placed at $R = 2.22$ m. The TSC Alfvén time is slowed down by choosing a mass enhancement factor of 50.0. The temperature of the vacuum region is chosen to be less than 1 eV, in order to prevent current from flowing outside the plasma region. The initial perturbation chosen to start the evolution of positional instability or VDE was a vertical displacement

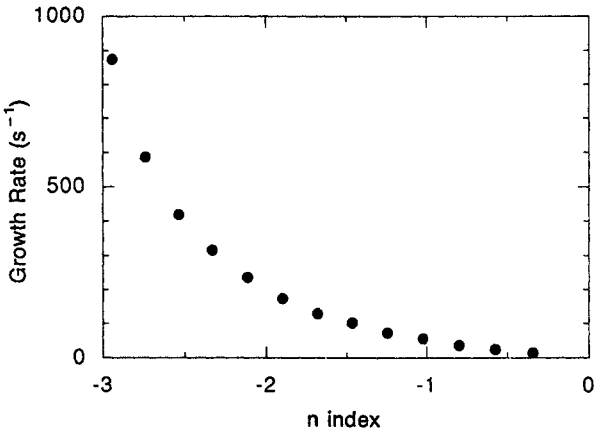

FIG. 3. Linear growth rate of JT-60U positional instability as a function of field decay index n. *The plasma current is 1.5 MA, the plasma current profile ℓ_i is 1.5 and the radial location of the magnetic axis is almost nominal, i.e.* R = *3.33 m. The triangularity of the plasma cross-section is very small, less than 0.1. For the case of sufficiently large magnetic field curvature, the growth rate tends asymptotically to the Alfvén frequency ($\gamma \sim 10^6$ s^{-1}). Observe here the non-linear dependence of the growth rate on the decay index* n *such that the more the decay index decreases, the more the growth rate of the positional instability rapidly increases.*

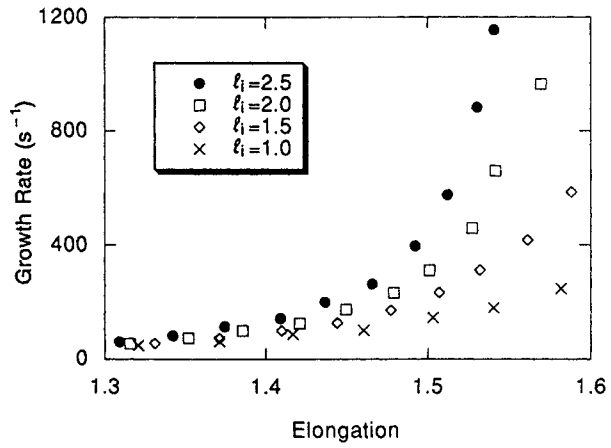

FIG. 4. Linear growth rate of JT-60U positional instability as a function of elongation of cross-section κ for various ℓ_i values. Peaked current profiles always give higher growth rates, reflecting less stability owing to an increase of effective plasma–wall distance.

of about 1 cm below the midplane of the vacuum vessel and was achieved by introducing a small amount of offset current of horizontal field coil.

3. FUNDAMENTAL CHARACTERISTICS OF JT-60U POSITIONAL STABILITY

In this section, we describe the TSC results that characterize JT-60U positional stability without any active feedback to provide a basis for the future discussion of JT-60U VDEs. The model assumed for the TSC positional stability analysis neglects the halo currents and decouples the plasma from all the poloidal field coils, similar to standard linear stability analysis based on a rigid plasma model [20].

Figure 2 shows a typical TSC simulation of the time evolution of a JT-60U positional instability for an elongated configuration with field decay index $n = -1.7$. Major plasma parameters are $I_p = 1.5$ MA, plasma internal inductance $\ell_i = 1.5$, cross-section elongation $\kappa = 1.4$, triangularity $\delta = 0.1$ and radial magnetic axis $R = 3.33$ m. Figure 2(a) indicates almost pure exponential growth of the vertical displacement of the magnetic axis. The linear growth rate γ is calculated to be 128 s^{-1}. Here, the initial offset of magnetic axis was 1.6 cm below the midplane. Throughout the entire time evolution, the elongation, triangularity and plasma current profile remained constant in time. Since a high plasma temperature was assumed in order to avoid Joule loss of the plasma current, the total plasma current remained unchanged. A 2-D plot of the poloidal flow vector field during the vertical motion is shown in Fig. 2(b). The dominant mode is a nearly rigid shift of the plasma cross-section. From these results, it is confirmed that the deformation during vertical displacement is negligibly small in JT-60U.

Figure 3 shows the linear growth rate as a function of the decay index n of the vertical field. Typical plasma parameters are $I_p = 1.5$ MA, $\ell_i = 1.5$ and $R = 3.33$ m. The plasma triangularity is very small (< 0.1). An important feature displayed in this figure is that the stabilizing effect of the JT-60U vacuum vessel depends strongly on the decay index, as predicted by the linear stability theory. For example, the standard configuration, $n = -0.9$, gives a small growth rate with $\gamma \approx 46$ s^{-1}. On the other hand, the elongated configuration with $n = -1.7$ (corresponding also to Fig. 2) gives a rather large growth of $\gamma \approx 128$ s^{-1}. In the case of a fictitious decay index of $n = -3.0$, the growth rate becomes about 1000 s^{-1}. The more the decay index decreases, the more the growth rate of positional instability rapidly increases, and finally, the growth rate becomes of the order of the poloidal Alfvén time-scale ($\sim 10^6$ s^{-1}). This nonlinear dependence of growth rate on the decay index

has an important consequence in the investigation of VDEs in JT-60U disruptive discharges discussed in the next section. Here, we briefly discuss this consequence: for a small n index degradation Δn originated from the eddy current effects, for example -0.3; the resultant increment of growth rate of positional instability is 80 s^{-1} for the elongated configuration ($n = -1.7$), while the increment for the standard configuration ($n = -0.9$) is only 19 s^{-1}. A degradation of decay index leads to an enhancement of positional instability growth rate, which depends strongly on the nominal n value of the unperturbed configuration. Through TSC simulation of VDEs, during the I_p quench phase, we will show that the value of Δn always becomes negative for vertically elongated plasma configurations, but for plasmas with nearly circular cross-sections the value of Δn can be slightly positive, which results in an improvement of stability with respect to vertical displacements. A detailed discussion about this will be given in the next section.

Figure 4 shows linear growth rates of vertical displacements as a function of plasma elongation for various ℓ_i values. The effect of destabilization due to peaking of the plasma current profile is evident. It is easily seen that elongation leads to high growth rate for all current profiles, as is predicted by the linear theory. For fixed elongation, peaking of the current profile results in higher growth rates. This implies that the stabilizing effect of the vacuum vessel is smaller for plasmas with more peaked current profiles, since the effective distance between the plasma and the vacuum vessel becomes larger. It seems that the destabilizing effect of the current peaking is most important at high elongation and that the current profile dependence disappears as the plasma configuration approaches that of a circle, as simple theory predicts.

Because bottom-diverted SN configurations in JT-60U have a large up/down asymmetry with regard to the midplane, it is interesting to study the positional stability characteristics of vertically elongated JT-60U plasma with SN divertors. Figure 5 shows the linear growth rate of vertical displacement versus initial equilibrium Z position of magnetic axis and the value of the decay index n at the initial magnetic axis. The plasma current profile was characterized by $\ell_i = 1.5$ and the elongation was $\kappa = 1.4$. The plasma current was 700 kA. As was predicted by the linear stability analysis [20], the linear growth rate of pure positional instability in the tokamak with a resistive shell is independent of plasma currents. The TSC result of Fig. 5 shows the reasonable dependence of the linear growth rates on the n indices that was previously displayed in Fig. 3. Closed cir-

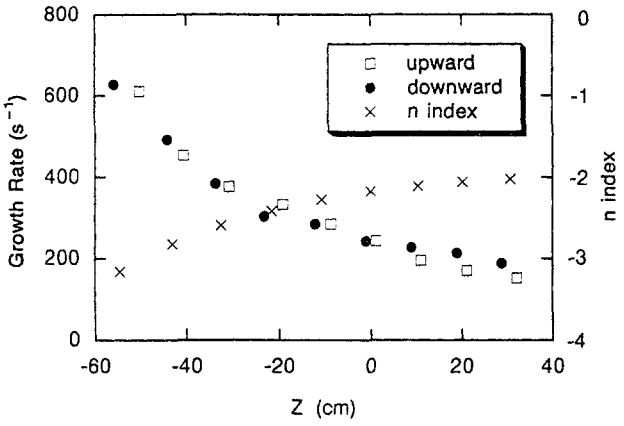

FIG. 5. Linear growth rate of vertical displacement versus initial Z position of the magnetic axis. The plasma current profile ℓ_i was assumed to be 1.5, the elongation was about $\kappa = 1.4$ and I_p was 700 kA. Closed circles denote downward displacement and open squares denote upward displacement. The growth rate increment at the lower position of the magnetic axis can reasonably be interpreted by the spatial distribution of the n index of the JT-60U SN divertor configuration with the help of Fig. 3. The distribution of n index values is due to the magnetic field structure of the JT-60U vertical field. There is no directional difference between upward and downward shifts as is predicted by the linear theory [20].

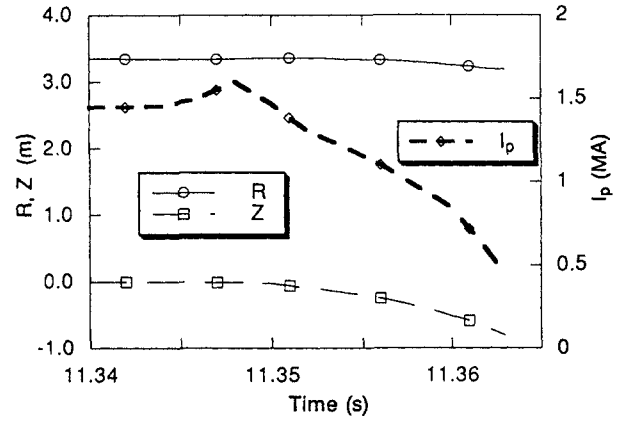

FIG. 6. Experimentally observed time evolutions of magnetic axis (R, Z) and plasma current in JT-60U disruptive shot 19 696 with the elongated configuration (n = −1.7). The predisruption value of plasma current was 1.5 MA. Energy quench occurred at t = 11.347 s within a period of about 200 μs. Almost no net halo current was observed within the period until t = 11.358 s. Control currents of all the poloidal field coils were kept almost constant in time until t = 11.36 s.

cles denote downward displacement and open squares denote upward displacement. Lower initial equilibrium positions give the highest growth rates because of the dependence of growth rate on field decay index n, consistent with Fig. 3. For example, the equilibrium with initial Z position of magnetic axis at -0.3 m feels a decay index $n = -2.5$ and gives rise to a growth rate γ of 400 s^{-1}, as is shown in both Figs 3 and 5. In the case of the nominal equilibrium ($Z = 0.0$ m), the magnetic field decay index $n = -2.2$ gives a growth rate of $\gamma = 260$ s^{-1}. A feature of Fig. 5 is that there is no difference of growth rate between upward and downward instabilities, as is predicted by the linear theory [20].

4. MECHANISM OF VDEs DURING PLASMA CURRENT QUENCH

In this section, firstly, the experimental results of a JT-60U disruptive discharge are described with special emphasis upon the correlation between the I_p quench rate and the VDE rate. Secondly, the experimentally observed VDE of a typical JT-60U disruptive discharge is reproduced via TSC simulation and then the mechanism of VDE during the I_p quench phase is investigated by using a simplified TSC model.

4.1. The experiment at JT-60U

The term VDE is phenomenological and describes the fast vertical shift of toroidal plasma during various kinds of tokamak disruption [3, 6]. Six types of disruption have been observed in the JT-60U experiment [8]:

(a) The density limit disruption commonly observed at any time during a discharge;
(b) The low ℓ_i disruption during the plasma current rampup;
(c) The high ℓ_i disruption during the plasma current rampdown with low plasma density;
(d) The vertical positional instability;
(e) The β_p collapse;
(f) The error field disruption.

Although disruptions can have different causes and involve a complex sequence of events, common features include a rapid energy quench and a resultant I_p quench, frequently coincident with fast vertical displacement. Figure 6 shows typical time evolutions of magnetic axis (R, Z) and plasma current in JT-60U disruptive shot 19 696, a density limit disruption. The plasma configuration was controlled by an equilibrium field with $n = -1.7$ and the predisruption value of plasma current was 1.5 MA. An energy quench occurred at $t = 11.347$ s and lasted for about 200 μs. It is assumed that the energy quench caused a flattening of the plasma current profile, and the flattening resulted in a small increase of total plasma current. In the final stage of current termination after $t = 11.36$ s, halo current up to 30% of total plasma current was induced in a halo region. However, almost no net halo current was observed during the period prior to $t = 11.358$ s. The control currents of all the poloidal field coils were kept almost constant in time until $t = 11.36$ s. Fast vertical displacement takes place during the I_p quench. The observed growth rate of the VDE (425 s^{-1}) was 3 to 4 times faster than the linear growth rate of vertical instability estimated as 128 s^{-1} in the previous section. Including the coupling effect of the plasma with the vacuum vessel, the observed I_p quench rate (52 s^{-1}) is consistent with the L/R time of a low T_e (<100 eV) plasma.

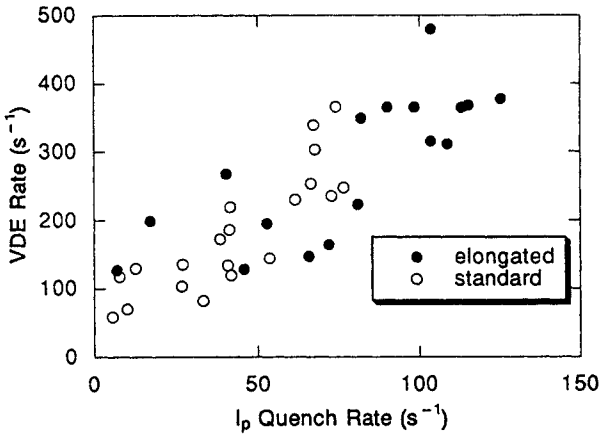

FIG. 7. VDE rate as a function of I_p quench rate in the JT-60U experiment. The open circles denote the standard configuration (n = −0.9) and the closed circles the elongated configuration (n = −1.7).

Data collected from many disruptive shots, including all six types of JT-60U disruption, indicate a close correlation between I_p quench rate and VDE rate. Figure 7 shows the experimental VDE rate as a function of I_p quench rate. Here, the experimental value of I_p quench rate γ_c^* is defined as the inverse of the time necessary for a 50% drop of plasma current. It is related to the usual rate γ_p, assuming exponential drop, by $\gamma_p = 0.69\gamma_c^*$. Data points with relatively low I_p quench rate correspond to density limit type disruptions, and relatively high I_p quench rates correspond to error field type disruptions. The predisrup-

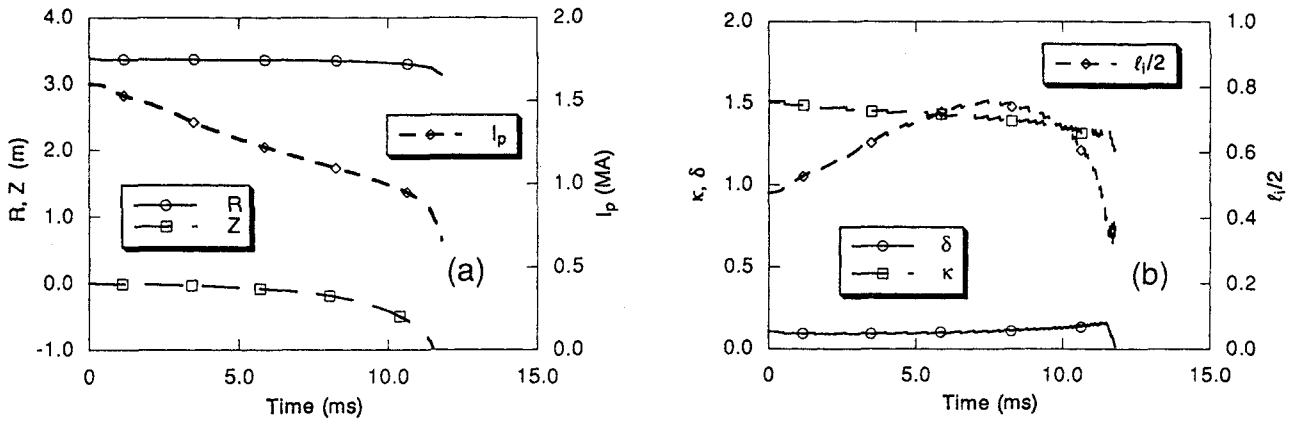

FIG. 8. TSC reproduction of VDE experiment 19 696 of Fig. 6. (a) The time trajectories of plasma current and magnetic axis (R, Z) in the case of the elongated configuration (n = −1.7). (b) Measured plasma current profile $\ell_i/2$, triangularity δ and elongation of cross-section κ. The parameters of predisruption such as plasma current, elongation, poloidal beta and internal inductance are the same as in JT-60U disruptive discharge 19 696. The effect of halo current is neglected. As for the discrepancy of trajectories between TSC and JT-60U experiments at the final phase after t = 11.0 ms, i.e. a large acceleration of VDE and a rapid I_p decrease of TSC, it is deduced that the experimentally observed halo current mitigates the fast VDE at the final stage of JT-60U disruptive discharge.

tion values of plasma current ranged from 1 to 3 MA and both the elongated ($n = -1.7$) and the standard ($n = -0.9$) configurations are included in Fig. 7. It is clear that the more the I_p quench rate increases, the more the VDE rate increases. These characteristic features of the experimental results are the subject of our TSC study described in Section 4.2.

4.2. Simulations using TSC

4.2.1. VDEs during I_p quench

Neglecting the effect of halo current, the nonlinear time evolution of a JT-60U VDE during the I_p quench phase was simulated using the TSC, starting from an initial state with a flattened plasma current profile caused by an energy quench of the core plasma. Figure 8(a) shows the TSC time trajectories of plasma current and magnetic axis position (R, Z). The TSC parameters of predisruption, such as plasma current, elongation, poloidal beta and internal inductance, are the same as for the JT-60U disruptive discharge 19 696. The electron temperature after the energy quench was specified so as to reproduce the experimental value of the I_p quench rate in the TSC simulation. The TSC estimate of T_e after energy quench is 100 eV, which is in reasonable agreement with the JT-60U ECE measurement. The TSC values of $\ell_i/2$ and elongation κ throughout the simulation are shown in Fig. 8(b). The elongation κ remains approximately constant, and the plasma current profile becomes gradually more peaked since plasma current is dissipated mainly in the low temperature peripheral region by its Joule loss. After the rearrangement of current profile, the plasma current decays with a slightly slower L/R decay time constant than the phase of the current profile relaxation. These characteristics of plasma current evolution nicely correspond to the experimental observations shown in Fig. 6. Notice again that the estimated VDE rate is 3.5 times higher than the linear growth rate of positional instability obtained in Section 3.

Figure 8 shows that the TSC model can reproduce the experimentally observed trajectories in the first half phase (until $t = 11.0$ ms after energy quench), and especially the vertical position. Aside from the final phase of disruption (after $t = 11.0$ ms), the TSC model appears to include all the essential mechanisms that can describe the actual VDE characteristics of the JT-60U disruption process. Our main interest in this paper lies in the interpretation and identification of enhanced VDEs due to I_p quenches by means of as simple a model as possible. The shrinkage of the plasma current channel is a contributing mechanism for VDEs [6]; however, it is easy to understand that the increase of $\ell_i/2$ shown in Fig. 8(b) is not sufficient to explain the rapid vertical displacement because the amount of enhancement of growth rate is estimated as only 50 s^{-1} from Fig. 4. In the following part of this section, we will discuss another VDE mechanism during the I_p quench phase. As for the discrepancy of

trajectories between the TSC model and the JT-60U experiment at the final phase after $t = 11.0$ ms, i.e. a large acceleration of VDE and a rapid I_p decrease of TSC, it is thought that the experimentally observed halo current mitigates the fast VDE at the final stage of JT-60U disruptive discharge.

4.2.2. VDE mechanism

In order to reveal the VDE mechanism of a current quenching plasma, we carried out a number of TSC analyses correlating the VDE rate and I_p quench rate for a variety of configurations including fictitious situations with $n = 0.0$, -2.1 and $n = -2.6$. Here, for computational convenience, the process of current profile relaxation was neglected by starting TSC simulation from a sufficiently relaxed initial state. As was mentioned before, this simple model is reasonable for investigating VDEs, because the ℓ_i change does not give the dominant effect in enhancing the VDE rate. A plasma current quench was induced by introducing a rapid T_e drop within 200 μs. Figure 9 displays the VDE rate as a function of I_p quench rate calculated by TSC. The main plasma parameters are $I_p = 1.5$ MA, $\ell_i = 1.5$ and elongations κ in the range between 1.1 and 1.5. In the figure, configurations of nearly circular cross-section ($n = 0.0$) and highly elongated cross-sections ($n = -2.1$, -2.6) were realized by introducing an artificial quadrupole magnetic field moment. During the TSC simulation, no significant change of elongation or plasma current profile was observed. It is clearly seen in Fig. 9 that the VDE rate depends strongly on the I_p quench rate. The values of VDE rate at the zero I_p quench rate correspond to growth rates of positional instability that are consistent with Fig. 3. The remarkable features of Fig. 9 are summarized as follows:

(a) The VDE rates of all the configurations increase as the I_p quench rate increases.

(b) An I_p quench causes a vertical displacement similar to a VDE even for nearly circular shaped plasmas, which should be marginally stable against both vertical displacement and radial expansive modes in the absence of an I_p quench.

(c) For highly elongated configurations ($n = -2.6$), an I_p quench substantially accelerates the VDEs compared with configurations with small elongation.

In order to investigate the VDE mechanism of current quenching plasmas, we measure the field decay index n at the magnetic axis in the TSC simulation and monitor the degradation of the field decay index Δn from its equilibrium value. The origin of Δn is an eddy current in the JT-60U vacuum vessel. For the case of an I_p quench rate of 40 s^{-1}, the amounts of degradation are $\Delta n = 0.0$ in circular shaped plasmas ($n = 0.0$), $\Delta n = -0.2$ in the standard configuration ($n = -1.0$), $\Delta n = -0.3$ both in the elongated configuration ($n = -1.7$) and in the fictitious case of $n = -2.1$, and $\Delta n = -0.4$ in the fictitious case of $n = -2.6$. The rapid current quench induces a large eddy current on the vacuum vessel. Especially for highly elongated configurations, eddy currents form in the top and bottom sections of the vacuum vessel, much more so than for circular shaped plasmas. These eddy currents produce an additional quadrupole moment of the magnetic field and result in the degradation of the field index. In Fig. 3 of Section 3, we discussed the fundamental characteristics of positional instability, where the strong dependence of linear growth rate on the field decay index n was shown. Now, it is clear that the

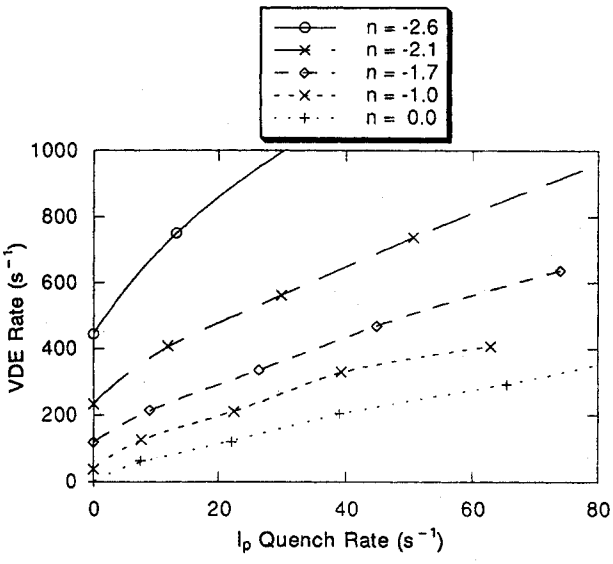

FIG. 9. VDE rate as a function of I_p quench rate by TSC. The VDE rates were estimated utilizing the very short trajectories of VDE evolutions starting from the initial equilibrium states (several centimetres of vertical shifts in most cases). Plasma current is 1.5 MA, current profile $\ell_i = 1.5$ and elongation κ lies in the range between 1.1 and 1.5. Observe that the VDE rate increases as I_p quench rate increases as in Fig. 7 and that I_p quench causes a vertical displacement similar to VDE even for nearly circularly shaped plasma. The values of VDE rate at the zero I_p quench rate correspond to the growth rates of pure positional instability.

degradation of field decay index n leads to a higher growth rate of positional instability. Although the magnitude of Δn is small for all configurations, i.e. at best $\Delta n = -0.4$ in the case of the fictitious configuration with $n = -2.6$, a substantial enhancement of the VDE can take place. For example, Fig. 3 shows that the resultant degradation of field index $\Delta n = -0.4$ provides an enhancement of growth rate of the positional instability of 450 s^{-1}. For this fictitious case, the linear growth rate of pure positional instability with no I_p quench is 430 s^{-1}, as can be seen in Fig. 3. From these considerations, we can identify a reasonable VDE mechanism as follows: the resultant growth rate of the VDE estimated by TSC (about 1100 s^{-1} from Fig. 9) consists of a pure positional instability (430 s^{-1}), an enhancement (450 s^{-1}) due to the degradation of field decay index $\Delta n = -0.4$ and a remaining enhancement ($\sim$ 200 s^{-1}), comparable in size with the VDE rate of a circular shaped configuration (shown in Fig. 9). At the end of this section, we will discuss another VDE mechanism due to unbalanced attractive forces caused by vacuum vessel asymmetries.

Now, let us proceed with a similar discussion of VDE enhancement in the other configurations. Although the current quench degrades the field index for the case of the elongated configuration of $n = -1.7$ and the case of the fictitious situation with $n = -2.1$ by approximately the same $\Delta n = -0.3$, the resultant destabilization is quite different. Figure 3 indicates that the resultant enhancements of linear growth rate are 150 s^{-1} for the case of $n = -2.1$ and 70 s^{-1} for the case of $n = -1.7$, respectively. Therefore, even if the degradations of field decay index Δn are the same, the VDEs of plasmas with higher elongations are more enhanced than the VDEs of plasmas with lower elongations. In fact, as one can see from Fig. 9, the discrepancy of enhanced VDE rate between them for the typical I_p quench rate of 40 s^{-1} is about 200 s^{-1}. Taking into account the difference in growth rate of pure positional instabilities between them, which can be seen from Fig. 3 to be 110 s^{-1}, the discrepancy of the enhanced VDE rate of 200 s^{-1} is reasonable, because the difference of the enhancement of positional instability due to the degradation of $\Delta n = -0.3$ can be estimated as 80 s^{-1}. For the standard configuration, the discrepancy of the enhanced VDE rate with the circular shaped plasma is about 100 s^{-1}. It consists of a portion of pure positional instability (40 s^{-1}) and an enhancement of VDE due to the degradation of $\Delta n = -0.2$ (20 s^{-1}). In the following, we attempt to interpret the effect on a VDE of an imbalance of attractive forces due to an asymmetric vacuum vessel.

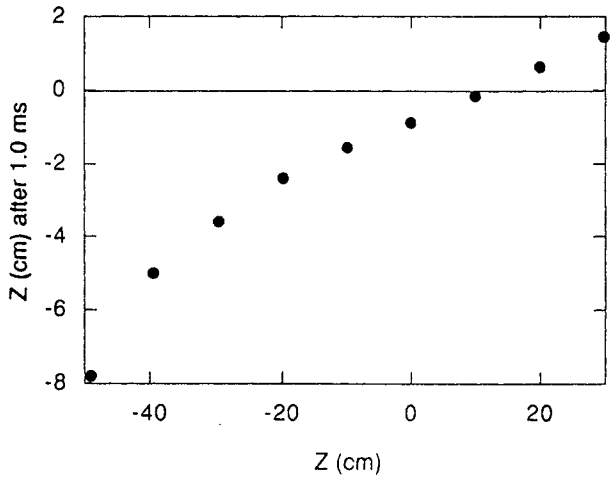

FIG. 10. Magnitudes of vertical displacement from initial Z position at 1.0 ms after energy quench. The predisruption values of the plasma current and the decay index of the equilibrium field were 700 kA and n = −2.0, respectively. There is a neutral position of the magnetic axis at 15 to 20 cm above the midplane, where the imbalance of the attractive force due to the up/down asymmetry of the JT-60U vacuum vessel can be cancelled.

4.2.3. Effect of an imbalance in attractive force

It remains to explain the TSC result that a circular shaped plasma, which should be marginally stable against both vertical displacement and radial expansion modes, also causes a VDE as was shown in Fig. 9. The degradation of field decay index Δn was very small (almost 0.0), and therefore this type of VDE is deduced not to be due to a positional instability. To clarify this mechanism, we investigated the plasma dynamics after the energy quench. Figure 10 shows the Z directional displacement of the magnetic axis 1.0 ms after energy quench. The predisruption values of the plasma current and the decay index of the equilibrium field were 700 kA and $n = -2.0$, respectively. In spite of the fact that the evolution of positional instability has no up/down directional dependence as was discussed in Section 3, even if there is no initial offset of magnetic axis for the perturbation, the VDE always evolves along the predestined direction, i.e. upward or downward. Figure 10 indicates that there is a neutral equilibrium location around 10 to 15 cm above the midplane in JT-60U tokamak, where the effective VDE rate can be zero, and above this neutral location the toroidal plasma is always attracted upward; below this neutral loca-

tion the plasma is always attracted downward. The speed of vertical shift becomes faster as the distance of the magnetic axis of the initial equilibrium from the neutral location increases. We obtained a similar directional dependence of vertical shift on the initial equilibrium for a circular shaped plasma, although circular shaped plasmas largely shift inward owing to the decrease of plasma current. It is clear that the VDE mechanism even of circular shaped plasmas is caused by the imbalance of attractive forces due to the up/down asymmetric distribution of eddy current on the vacuum vessel. As was mentioned, the vacuum vessel in the JT-60U tokamak is egg shaped, and the lower part of the cross-section is slightly deformed on the inside. Therefore, the indication of a neutral equilibrium location of 10 to 15 cm from Fig. 10 is reasonable, and this has also been experimentally demonstrated [21].

It is important to note that there can be a neutral equilibrium location in any tokamak device, such that one can always partly suppress a VDE during an I_p quench. In the case of a completely up/down symmetric shell, the neutral equilibrium location lies on the midplane of the vacuum vessel.

5. CONCLUSIONS

With a view to adding to our understanding of disruptions so that we can operate with disruption-free discharges, or at least avoid hard disruptions by soft landing, mechanisms that govern VDEs during I_p quenches in JT-60U disruptive discharges have been investigated using the TSC.

Firstly, the fundamental characteristics of JT-60U positional instability were investigated to gain insight into the observed VDE phenomena and to identify VDE mechanisms in the JT-60U tokamak. Utilizing the remodelled JT-60U vacuum vessel, realistic TSC simulations of JT-60U current quench disruptions were carried out in a self-consistent manner including the stabilizing effect of the conducting shell and the deformation of the plasma. The TSC results show that the plasma deformation is not large during the positional instability since the nominal configuration of JT-60U has only a mildly elongated cross-section. Linear growth rates of positional instability were evaluated and the dependence of linear growth rate on both the magnitude of the field decay index n and the initial equilibrium Z position of the magnetic axis was clarified. The effect of plasma current profile shape on linear growth rate, which reflects the effective plasma–wall distance, was also evaluated quantitatively. It was also shown that there is no directional dependence of the linear growth rate on upward or downward shifts in spite of an up/down asymmetry of equilibrium fields, owing to the bottom-diverted SN configuration.

Secondly, non-linear evolutions of plasma displacement interacting with the vacuum vessel were studied numerically using TSC. Experimentally observed fast VDEs with growth rates 3 or more times higher than is predicted by positional stability theory were reproduced well by the TSC simulations especially during the first half phase of the disruption process. It was clarified that the rapid I_p quench can accelerate vertical displacement owing to both the up/down asymmetry of the eddy current distribution originated from the asymmetric geometry of the JT-60U vacuum vessel and the degradation of field decay index n leading to high growth rate of positional instability. It was found that the degradation of field decay index originating in the large induced eddy currents due to the rapid I_p quench can accelerate VDEs and must be added to the list of previously proposed mechanisms for explaining VDEs, such as the asymmetry of attractive force, the shrinkage of plasma boundary or the peaking of plasma current profile, and the stronger imbalance of stabilizing/destabilizing force produced during current quench phase. For the standard configuration ($n = -0.9$), the asymmetry of attractive force on the toroidal plasma is a dominant mechanism of the VDE. For the elongated configuration ($n = -1.7$), the degradation of field decay index n plays an important role in addition to the asymmetry of the attractive force. Although the degradation of field decay index due to the I_p quench is similar for both the standard and the elongated configurations, the resultant destabilization of VDEs is quite different; the elongated equilibrium is much more unstable than the standard elongation. It was shown that the VDE characteristics of highly elongated configurations with rapid I_p quench can be dominated by the field decay index degradation.

The newly identified VDE mechanisms in disruptive discharges have significant implications for tokamak reactor design. For example, in ITER with a high inductance superconducting PF coil system, the quadrupole component of the shaping field cannot be ramped down during a disruption at the same rate as the I_p decay. Even if it were possible, the control gain of the feedback loop must be high enough, and high gain loops require high cost power supplies. Therefore, the mechanism described in this paper

can be expected to occur during the current decay phase, and the plasma will always become positionally unstable at a higher growth rate than the predisruption value. This suggests that the design guidelines for next generation tokamaks must be conservative against the allowable plasma elongation. To suppress the VDE during disruption, the magnetic field curvature should be less than some limit, i.e. one cannot necessarily adopt the plasma configuration with a highly elongated cross-section, at the sacrifice of a favourable elongation for better confinement characteristics without considerding the impact of disruptions. Another possible approach to soften VDEs is to optimize the vertical position of the plasma equilibrium to cancel out the unbalanced force due to the up/down asymmetry of the conducting wall geometry.

Here, we propose design and control strategies for next generation tokamaks without fast VDEs or hard disruptions. The first strategy is a careful optimization of allowable plasma elongation. The second is a softening of current quenches by mitigation of the energy quench, which has already been demonstrated in the JT-60U experiment, and position control optimization so as to minimize the imbalance of the attractive forces on the toroidal plasma during the I_p quench. Up/down symmetry of the vacuum vessel geometry with regard to the midplane is favourable, otherwise, the effort of further control optimization is necessary to find the best location of the magnetic axis in order to minimize the imbalance of attractive forces.

We have discussed in detail only the VDE mechanism in JT-60U I_p quenches during the first half phase of the disruption process when halo current is almost absent. Halo current appears in the open flux SOL especially during the last half phase of disruption. With regard to VDE suppression due to halo current, Sayer et al. have investigated the halo effect in disruptions and have demonstrated excellent agreement between TSC simulation and DIII-D experiments [2]. From the engineering viewpoint of the fusion reactor design, the more refined VDE model, which includes halo current effects for the entire disruption process, is a critical matter.

ACKNOWLEDGEMENTS

The authors wish to thank the members of the Japan Atomic Energy Research Institute who have contributed to the JT-60U project, and are indebted to colleagues from the JT-60U group for making their data freely available. They are most grateful to Dr. H. Ninomiya for his continuous encouragement. Useful discussions with Dr. S. Tokuda of JAERI and Prof. T. Takeda of the University of Electro-Communications, Tokyo, are also acknowledged.

REFERENCES

[1] YOSHINO, R., et al., Nucl. Fusion **33** (1993) 1599.
[2] SAYER, R.O., et al., Nucl. Fusion **33** (1993) 969.
[3] YOSHINO, R., et al., in Plasma Physics and Controlled Nuclear Fusion Research 1994 (Proc. 15th Int. Conf. Seville, 1994), Vol. 1, IAEA, Vienna (1995) 685.
[4] MERRILL, B.J., JARDIN, S.C., Fusion Eng. Des. **5** (1987) 235.
[5] SAYER, R.O., et al., Bull. Am. Phys. Soc. **33** (1988) 1972.
[6] GRUBER, O., et al., Plasma Phys. Control. Fusion **34** (1993) B191.
[7] THOMAS, P.R., et al., in Plasma Physics and Controlled Nuclear Fusion Research 1984 (Proc. 10th Int. Conf. London, 1984), Vol. 1, IAEA, Vienna (1985) 353.
[8] YOSHINO, R., et al., J. Plasma Fusion Res. **70** (1994) 1081.
[9] NEYATANI, Y., et al., Fusion Technol. **28** (1995) 1634.
[10] JARDIN, S.C., et al., J. Comput. Phys. **66** (1986) 481.
[11] HUMPHREYS, D.A., YOSHINO. R., JT-60 Upgrade Vertical Stability Experiments and Analysis, Rep. JAERI-M 92-069, Japan Atomic Energy Research Inst., Tokyo (1992).
[12] JARDIN, S.C., et al., Nucl. Fusion **27** (1987) 569.
[13] SAYER, R.O., et al., TSC Disruption Scenarios and CIT Vacuum Vessel Force Evolution, Rep. ORNL/FEDC-89/3, Oak Ridge Natl Lab., TN (1990).
[14] JARDIN, S.C., et al., Nucl. Fusion **33** (1993) 371.
[15] WARD, D.J., JARDIN, S.C., Nucl. Fusion **32** (1992) 973.
[16] WARD, D.J., HOFMANN, F., Nucl. Fusion **34** (1994) 401.
[17] LISTER, J.B., et al., Nucl. Fusion **30** (1990) 2349.
[18] KELLMAN, A.F., et al., in Fusion Technology (Proc. 16th Symp. London, 1990), Vol. 2, Pergamon Press, Oxford (1991) 1045.
[19] PICK, M.A., et al., in Fusion Engineering (Proc. 14th Symp. San Diego, 1991), Vol. 1, IEEE, New York (1992) 187.
[20] FUKUYAMA, A., et al., Jpn. J. Appl. Phys. **14** (1975) 871.
[21] YOSHINO, R., et al., Nucl. Fusion **36** (1996) 295.

(Manuscript received 6 April 1995
Final manuscript accepted 18 September 1995)